LETTER • OPEN ACCESS

Radiance-based NIR$_v$ as a proxy for GPP of corn and soybean

Environmental Research Letters

CrossMark

LETTER

Radiance-based NIR$_v$ as a proxy for GPP of corn and soybean

Genghong Wu[1,2] ⓘ, Kaiyu Guan[1,2,3,11] ⓘ, Chongya Jiang[1,2,11] ⓘ, Bin Peng[1,3] ⓘ, Hyungsuk Kimm[1] ⓘ,
Min Chen[4], Xi Yang[5], Sheng Wang[1,2], Andrew E Suyker[6], Carl J Bernacchi[2,7,8] ⓘ, Caitlin E Moore[2,8] ⓘ,
Yelu Zeng[9], Joseph A Berry[9] and M Pilar Cendrero-Mateo[10] ⓘ

[1] College of Agricultural, Consumer and Environmental Sciences, University of Illinois at Urbana Champaign, Urbana, Illinois, United States of America
[2] Center for Advanced Bioenergy and Bioproducts Innovation, University of Illinois at Urbana Champaign, Urbana, Illinois, United States of America
[3] National Center of Supercomputing Applications, University of Illinois at Urbana-Champaign, Urbana, Illinois, United States of America
[4] Joint Global Change Research Institute, Pacific Northwest National Laboratory, College Park, Maryland, United States of America
[5] Department of Environmental Sciences, University of Virginia, Charlottesville, Virginia, United States of America
[6] School of Natural Resources, University of Nebraska-Lincoln, Lincoln, Nebraska, United States of America
[7] Global Change and Photosynthesis Research Unit, USDA-ARS, Urbana, Illinois, United States of America
[8] Department of Plant Biology, University of Illinois at Urbana-Champaign, Urbana, Illinois, United States of America
[9] Department of Global Ecology, Carnegie Institution for Science, Stanford, California, United States of America
[10] Laboratory for Earth Observation, Image Processing Laboratory, University of Valencia, Spain
[11] Authors to whom any correspondence should be addressed.

E-mail: kaiyug@illinois.edu and chongya@illinois.edu

Abstract

Substantial uncertainty exists in daily and sub-daily gross primary production (GPP) estimation, which dampens accurate monitoring of the global carbon cycle. Here we find that near-infrared radiance of vegetation (NIR$_{v,Rad}$), defined as the product of observed NIR radiance and normalized difference vegetation index, can accurately estimate corn and soybean GPP at daily and half-hourly time scales, benchmarked with multi-year tower-based GPP at three sites with different environmental and irrigation conditions. Overall, NIR$_{v,Rad}$ explains 84% and 78% variations of half-hourly GPP for corn and soybean, respectively, outperforming NIR reflectance of vegetation (NIR$_{v,Ref}$), enhanced vegetation index (EVI), and far-red solar-induced fluorescence (SIF$_{760}$). The strong linear relationship between NIR$_{v,Rad}$ and absorbed photosynthetically active radiation by green leaves (APAR$_{green}$), and that between APAR$_{green}$ and GPP, explain the good NIR$_{v,Rad}$-GPP relationship. The NIR$_{v,Rad}$-GPP relationship is robust and consistent across sites. The scalability and simplicity of NIR$_{v,Rad}$ indicate a great potential to estimate daily or sub-daily GPP from high-resolution and/or long-term satellite remote sensing data.

1. Introduction

Monitoring and quantifying terrestrial photosynthesis from satellite remote sensing is crucial for understanding the global carbon cycle. Either process-based models (Jiang and Ryu 2016, Chen *et al* 2019) or more empirical models (Running *et al* 2004, Jung *et al* 2011) have been widely used for regional or global gross primary production (GPP) estimations. Process-based models employ complex model structure, while existing empirical models rely on various imposed functions. Uncertainties in climate forcing and model parametrization lead to largely diverged GPP estimation regarding the total amount and spatio-temporal patterns (Anav *et al* 2015, Ryu *et al* 2019). Particularly, GPP estimation at short time scales (e.g. sub-daily and daily) is still challenging (Bodesheim *et al* 2018, Wang *et al* 2019). Effective and parsimonious ways to estimate GPP with low dependence on climate forcing and model parameterization are highly required.

Recent advances in satellite-based solar-induced fluorescence (SIF) monitoring capabilities may

Table 1. Site and observation information. GPP observations are available year-round for all site-years.

Site	Year	Crop	Growing season	Hyperspectral	SIF	APAR$_{green}$
UIUC (rainfed)	2016	Soybean	May 17–Oct 17	Aug 7–Sep 25	Aug 7–Sep 25	NA
	2017	Corn	May 16–Oct 30	Jun 6–Oct 2	Jun 6–Oct 2	NA
	2018	Corn	May 8–Oct 8	Jun 28–Oct 8	Jun 28–Oct 8	NA
UNL2 (irrigated)	2017	Corn	May 8–Oct 30	Jul 15–Oct 15	Jul 15–Oct 15	Jun 2–Oct 15
	2018	Soybean	May 14–Oct 19	Jun 19–Oct 14	Jul 19–Oct 14	Jun 7–Oct 14
UNL3 (rainfed)	2017	Corn	May 8–Oct 30	Jul 15–Sep 17	Jul 15–Oct 15	Jun 2–Oct 15
	2018	Soybean	May 14–Oct 19	Jul 8–Oct 14	Jul 8–Oct 14	Jun 7–Oct 14

provide a new opportunity for GPP estimation. Although SIF has been reported as a better proxy for photosynthesis at leaf (Baker 2008), landscape (Li *et al* 2018), and global (Guanter *et al* 2014) scales than traditional GPP proxies such as enhanced vegetation index (EVI) (Sims *et al* 2006), divergent SIF-GPP relationships have been obtained from ground-based observations (Damm *et al* 2015, Yang *et al* 2015, Miao *et al* 2018). Such divergent SIF-GPP relationships may stem from complex links between fluorescence emission efficiency and photosynthetic efficiency (Porcar-Castell *et al* 2014) as well as impacts of canopy structure related to reabsorption and scattering processes (Yang *et al* 2018b, van der Tol *et al* 2019). The coarse resolution (Frankenberg *et al* 2011, Joiner *et al* 2013) or short temporal coverage (Sun *et al* 2017, Köhler *et al* 2018, Li and Xiao 2019) of SIF datasets further restrict the application of SIF for GPP estimation.

A new vegetation index, near-infrared reflectance of vegetation (NIR$_{v,Ref}$), could open up a new opportunity to quantify GPP. NIR$_{v,Ref}$, defined as the product of normalized difference vegetation index (NDVI) and NIR reflectance (NIR$_{Ref}$), is found accounting for canopy structure well and photosynthetic capacity to some extent (Badgley *et al* 2017). Without any other auxiliary information, NIR$_{v,Ref}$ has been reported to explain 68% of FLUXNET GPP variation at monthly to annual time scales (Badgley *et al* 2019). However, the relationship between NIR$_{v,Ref}$ and GPP at shorter time scales (sub-daily to daily) has not been investigated yet, and that relationship is expected to be poorer than at monthly scale, as NIR$_{v,Ref}$ has much smaller variations at short time scales. Considering that radiances can be used in studies with variable light (Badgley *et al* 2017), observed NIR$_{Ref}$ in NIR$_v$ can be replaced with observed NIR radiance (NIR$_{Rad}$) to derive a new proxy NIR$_{v,Rad}$, which takes the incoming radiation into account (Zeng *et al* 2019) and has the potential to be a better proxy for GPP at short time scales. However, the relationship between NIR$_{v,Rad}$ and GPP has not been investigated and its potential awaits to be evaluated.

The objective of this study is to evaluate whether NIR$_{v,Rad}$ is a better proxy of GPP than NIR$_{v,Ref}$ and SIF for corn and soybean, two major crops in the US Corn Belt. For a comprehensive assessment of the relationships between GPP and those proxies, we integrated a range of field observations including hyperspectral

radiance and reflectance, far-red SIF, GPP flux, and canopy light absorption at half-hourly interval over seven site-years. The overachieving questions that we aim to address are: How is NIR$_{v,Rad}$'s ability to estimate GPP compared with other widely used recognized proxies (NIR$_{v,Ref}$, EVI and SIF) for corn and soybean, and what factors may lead to a better performance of NIR$_{v,Rad}$? We propose the following three hypotheses. First, we hypothesize that the relationship between NIR$_{v,Rad}$ and GPP is the strongest compared to three other widely recognized proxies (NIR$_{v,Ref}$, EVI and SIF), especially at short time scales. Second, we hypothesize that the strong relationship between NIR$_{v,Rad}$ and GPP can be explained by the fact that NIR$_{v,Rad}$ better accounts for photosynthetically active radiation (PAR) absorbed by green leaves (APAR$_{green}$). Third, we hypothesize that the relationship between NIR$_{v,Rad}$ and GPP for soybean (C3 crop) or corn (C4 crop) is site-independent. We suggest these features might make NIR$_{v,Rad}$ a better proxy for estimating GPP in the US Corn Belt than NIR$_{v,Ref}$, EVI and SIF.

2. Materials and methods

2.1. Study site

This study was conducted at three agricultural sites in the US Corn Belt. One rainfed site was located at the Energy Farm of University of Illinois at Urbana-Champaign (UIUC, 40.0628 °N, 88.1959 °W). Another two sites were located at the Eastern Nebraska Research and Extension Center of University of Nebraska-Lincoln, with one irrigated (UNL irrigated, 41.1649 °N, 96.4701 °W) and one rainfed (UNL rainfed, 41.1797 °N, 96.4397 °W) site. The mean annual temperature and precipitation over the period of 1990–2018 were (11.5 °C, 1036 mm) and (10.1 °C, 770 mm) at UIUC (Willard Airport weather station) and two UNL sites (National Climate Data Center, Nebraska, Mead 6 S weather station), respectively. The UIUC site had a corn-corn-soybean rotation, whereas the two UNL sites were corn-soybean rotation. The growing season (from planting to harvesting) was generally May–October for both crops across all the three sites. During 2016–2018, a total of four and three site-year observations were made for corn and soybean, respectively. Detailed site and observation information are summarized in table 1.

2.2. Fluospec2 system and derivation of vegetation indices and SIF

Fluospec2 systems (Yang *et al* 2018a, Miao *et al* 2018) were installed to acquire vegetation indices and SIF. Each Fluospec2 system included two subsystems for SIF and hyperspectral data collection separately. The SIF subsystem employed a QE Pro spectrometer (Ocean Optics Inc., USA) covering 730–780 nm with a spectral resolution of 0.15 nm. The hyperspectral subsystem employed a HR2000+ spectrometer (Ocean Optics Inc., USA) covering 400–1100 nm with a spectral resolution of 1.1 nm. Each subsystem had two fibers collecting downwelling irradiance and upwelling radiance. Details of Fluospec2 system and data acquisition can be found in supplementary methods which is available online at stacks.iop.org/ERL/15/034009/mmedia.

$NIR_{v,Ref}$, $NIR_{v,Rad}$ and EVI were calculated from the Fluospec2 system:

$$NDVI = \frac{NIR_{Ref} - Red_{Ref}}{NIR_{Ref} + Red_{Ref}} \tag{1}$$

$$NIR_{v,Ref} = NIR_{Ref} \times NDVI \tag{2}$$

$$NIR_{v,Rad} = NIR_{Rad} \times NDVI \tag{3}$$

$$EVI = 2.5 \times \frac{NIR_{ref} - Red_{ref}}{NIR_{ref} + 6 \times Red_{ref} - 7.5 \times Blue_{ref} + 1} \tag{4}$$

where the average of 770–780 nm, 650–660 nm, and 460–470 nm were used for NIR, Red and Blue band, respectively. SIF at 760 nm (SIF_{760}) was retrieved from the SIF subsystem using the improved Fraunhofer Line Depth method (Alonso *et al* 2008, Cendrero-mateo *et al* 2019), which used the whole downwelling irradiance (E) and upwelling radiance (L) spectrum information from 745 to 780 nm to extract the SIF signal.

$$SIF_{760} = \frac{\alpha_R \times E(\lambda_{out}) \times L(\lambda_{in}) - L(\lambda_{out}) \times E(\lambda_{in})}{\alpha_R \times E(\lambda_{out}) - \alpha_F \times E(\lambda_{in})}, \tag{5}$$

where α_R and α_F are correction factors to account for the non-linear variation of reflectance (R) and fluorescence (F) inside (λ_{in}) and outside (λ_{out}) the O_2-A absorption band at wavelength λ, respectively. Detailed SIF data processing can be found in supplementary methods.

2.3. Eddy covariance (EC) system and derivation of GPP

EC systems were installed to acquire net ecosystem exchange (NEE), and GPP was estimated based on standard night-time partitioning algorithms (Reichstein *et al* 2005). Each EC system consisted of a sonic anemometer (81000VRE, R.M. Young Inc., USA for the UIUC site; R3, Gill Instruments Inc., UK for the two UNL sites) and a CO_2/H_2O infrared gas analyzer (LI-7500 and LI-7200, LI-COR Inc., USA for the UIUC site and the two UNL sites, respectively). Raw 10 Hz

Carbon fluxes data collected from EC systems were processed to derive half-hourly NEE. Detailed information on site instrumentation can be found in (Zeri *et al* 2011) for UIUC site, and in (Suyker and Verma 2012) for UNL sites. Detailed EC data processing can be found in supplementary methods.

2.4. Ancillary data

Downwelling and upwelling PAR were measured above and below canopy by multiple point or line quantum sensors (LI-COR Inc., USA), from which the fraction of absorbed PAR (FPAR) were derived at half-hourly interval. Leaf area index (LAI) were measured from destructive samples at an interval of 10–14 d, and green leaves were separated from yellow leaves to provide green area index (GAI) measurements. The ratio of GAI to LAI were linearly interpolated and half-hourly $APAR_{green}$, light use efficiency of green leaves (LUE_{green}) (Gitelson and Gamon 2015) and fluorescence yield (LUE_f) were then calculated as:

$$APAR_{green} = PAR \times FPAR \times \frac{GAI}{LAI} \tag{6}$$

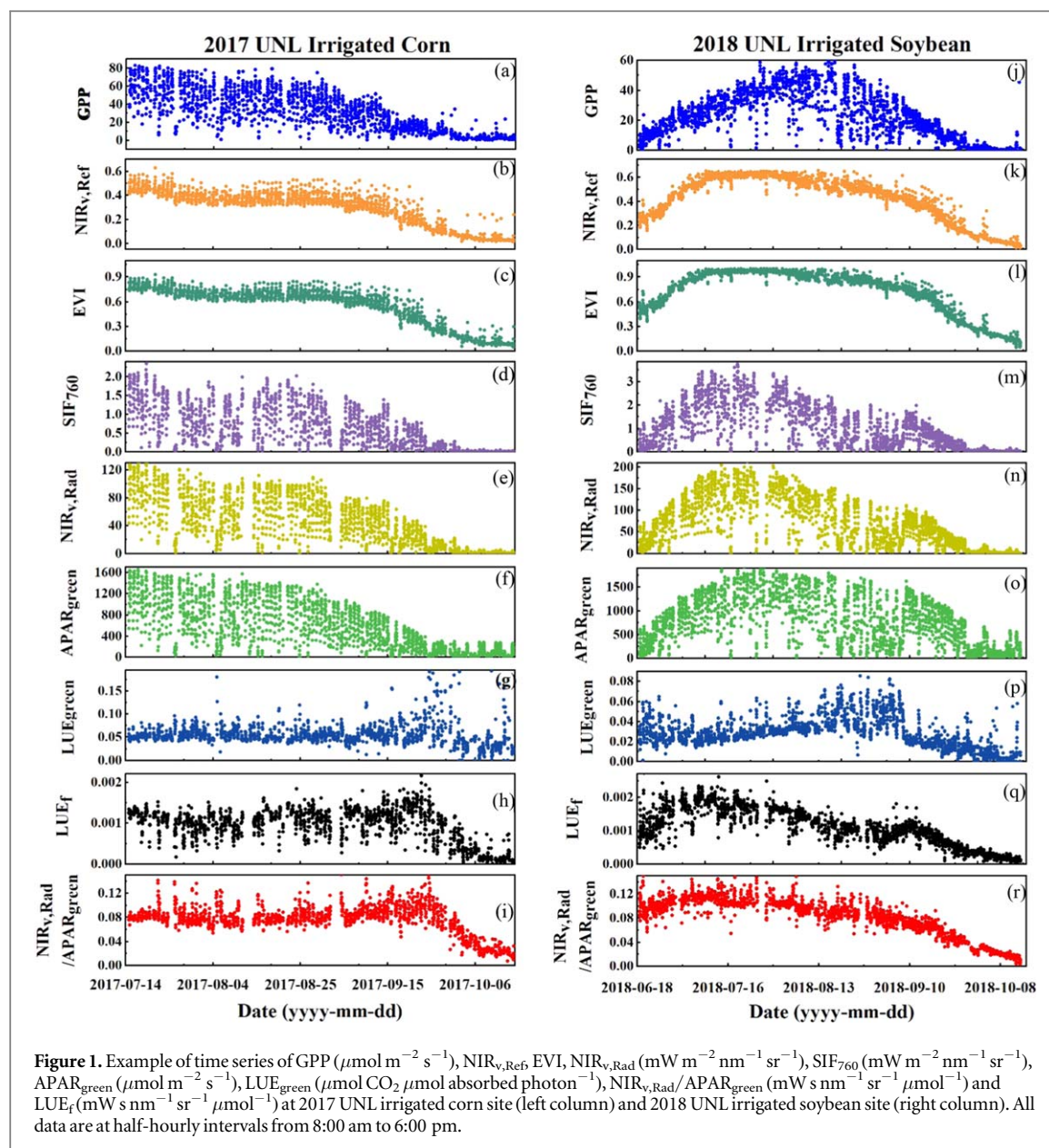$$LUE_{green} = \frac{GPP}{APAR_{green}} \tag{7}$$

$$LUE_f = \frac{SIF_{760}}{APAR_{green}}. \tag{8}$$

These data were only acquired at the two UNL sites.

2.5. Data analysis

To test the first hypothesis, the relationships between GPP and its four proxies, $NIR_{v,Ref}$, EVI, $NIR_{v,Rad}$, and SIF_{760} were investigated. All site-year data for each species were combined in this analysis. Investigations were conducted at three time scales (half-hourly, daily, and monthly). Because of uncertainties under low light conditions in the early morning and late afternoon, only data from 8:00 am to 6:00 pm (local standard time) were used. Therefore, daily data averaged from half-hourly data were daytime means in the strict sense. Only days with data gaps less than 25% were used. Monthly mean data were calculated for months with at least 10 days of available data. Linear regression of GPP-$NIR_{v,Rad}$ and GPP-SIF_{760} were established with zero intercepts, considering the fact that there is no photosynthesis when radiation is zero. For linear regression of GPP-$NIR_{v,Ref}$ and GPP-EVI, the intercept term was employed because these two proxies do not reach zero.

To test the second hypothesis, the relationships between the four proxies and $APAR_{green}$ were also evaluated at the three time scales at the two UNL sites, where $APAR_{green}$ data were available. Similar to LUE_{green} and LUE_f, we divided $NIR_{v,Rad}$ by $APAR_{green}$ and then examined the relationship between LUE_{green} and $NIR_{v,Ref}$, EVI, LUE_f, $NIR_{v,Rad}/APAR_{green}$ at half-hourly, daily and monthly scales. Coefficient of determination (R^2) was used to quantify their relationships.

Figure 1. Example of time series of GPP (μmol m^{-2} s^{-1}), NIR$_{v,Ref}$, EVI, NIR$_{v,Rad}$ (mW m^{-2} nm^{-1} sr^{-1}), SIF$_{760}$ (mW m^{-2} nm^{-1} sr^{-1}), APAR$_{green}$ (μmol m^{-2} s^{-1}), LUE$_{green}$ (μmol CO$_2$ μmol absorbed photon^{-1}), NIR$_{v,Rad}$/APAR$_{green}$ (mW s nm^{-1} sr^{-1} μmol^{-1}) and LUE$_f$ (mW s nm^{-1} sr^{-1} μmol^{-1}) at 2017 UNL irrigated corn site (left column) and 2018 UNL irrigated soybean site (right column). All data are at half-hourly intervals from 8:00 am to 6:00 pm.

To test the third hypothesis, site-specific GPP-NIR$_{v,Rad}$ relationship was investigated separately for corn and soybean. Half-hourly data were used for this analysis. For each crop type and each site, the linear relationship between GPP and NIR$_{v,Rad}$ was established, and the slopes across sites were compared. Subsequently, linear models calibrated from one site were applied to the remaining two sites to predict GPP, i.e. NIR$_{v,Rad}$-derived GPP. The NIR$_{v,Rad}$-derived GPP was compared with EC-derived GPP. Root mean square error (RMSE) was used to evaluate the performance of the GPP prediction.
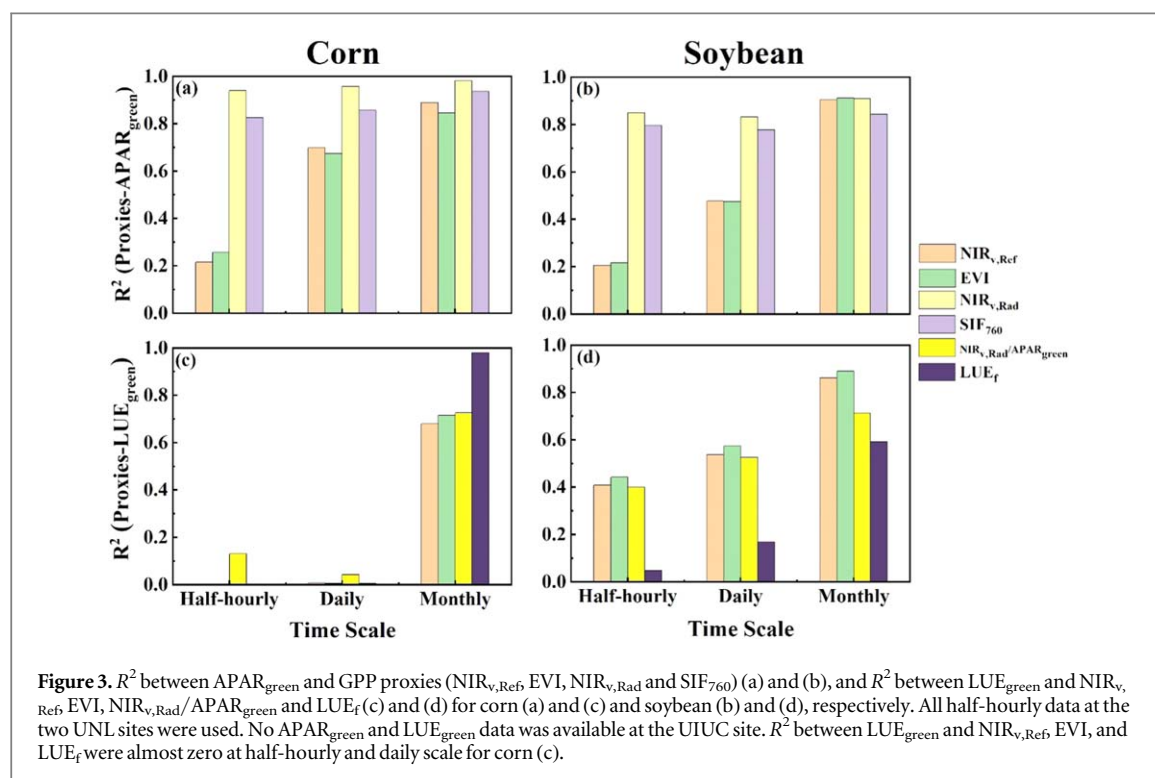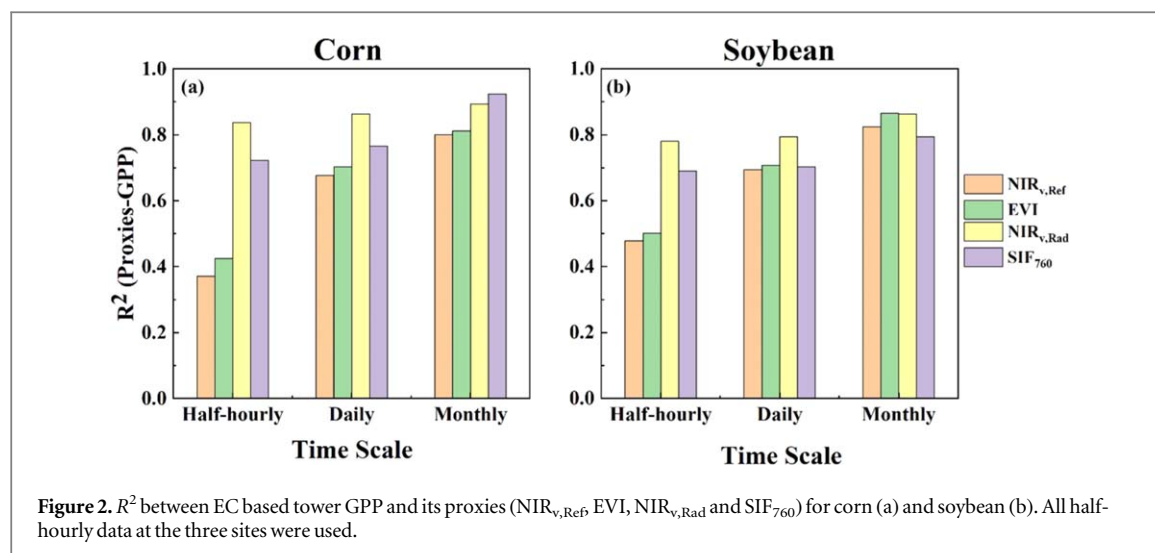
3. Results

3.1. Relationship between GPP and its proxies
Overall, GPP, NIR$_{v,Ref}$, EVI, NIR$_{v,Rad}$ and SIF$_{760}$ followed similar seasonal trajectories (figure 1). Peak GPP was higher for corn than for soybean. NIR$_{v,Ref}$, EVI, and APAR$_{green}$ were similar between corn and soybean, but SIF$_{760}$ and NIR$_{v,Rad}$ were lower for corn than soybean. LUE$_{green}$, LUE$_f$ and NIR$_{v,Rad}$/APAR$_{green}$ displayed weak seasonal variation, especially after excluding the senescence period (e.g. from late September to October) when the derivations of FPAR$_{green}$ and subsequently LUE$_{green}$ were prone to uncertainties (Gitelson *et al* 2018).

NIR$_{v,Ref}$-GPP relationship varied with time scales for both corn and soybean, and it tended to be stronger scaled with temporal aggregation (figure 2). From half-hourly to monthly, R^2 of NIR$_{v,Ref}$-GPP increased from 0.37 to 0.80 for corn and from 0.48 to 0.83 for soybean. The EVI-GPP relationship also showed a similar time scale-dependent pattern. In contrast, both NIR$_{v,Rad}$ and SIF$_{760}$ showed more consistent performance at different time scales. R^2 differences of NIR$_{v,Rad}$-GPP relationship between monthly scale and

Figure 2. R^2 between EC based tower GPP and its proxies ($NIR_{v,Ref}$, EVI, $NIR_{v,Rad}$ and SIF_{760}) for corn (a) and soybean (b). All half-hourly data at the three sites were used.

Figure 3. R^2 between $APAR_{green}$ and GPP proxies ($NIR_{v,Ref}$, EVI, $NIR_{v,Rad}$ and SIF_{760}) (a) and (b), and R^2 between LUE_{green} and $NIR_{v,Ref}$, EVI, $NIR_{v,Rad}/APAR_{green}$ and LUE_f (c) and (d) for corn (a) and (c) and soybean (b) and (d), respectively. All half-hourly data at the two UNL sites were used. No $APAR_{green}$ and LUE_{green} data was available at the UIUC site. R^2 between LUE_{green} and $NIR_{v,Ref}$, EVI, and LUE_f were almost zero at half-hourly and daily scale for corn (c).

half-hourly scale were only 0.06 and 0.08 for corn and soybean, respectively.

Among the four GPP proxies, $NIR_{v,Rad}$ exhibited the strongest relationship with GPP at short time scales (half-hourly and daily) for both corn and soybean (figure 2), which confirmed our first hypothesis. Overall, $NIR_{v,Rad}$ explained 84%, 86% and 89% of the variation of corn GPP at half-hourly, daily and monthly scales, respectively. Slightly lower values were achieved for soybean GPP, with 78%, 79% and 86% of the variation explained at half-hourly, daily and monthly scales, respectively. In particular, at daily scale which is of concern for crop growth monitoring, $NIR_{v,Rad}$ better explained the variation of GPP compared to other three proxies. For corn, the portion of GPP variation explained by $NIR_{v,Rad}$ was 19%, 16%

and 10% higher than $NIR_{v,Ref}$, EVI and SIF_{760}, respectively. For soybean, this portion was 10%, 9% and 9% higher than $NIR_{v,Ref}$, EVI and SIF_{760}, respectively.

3.2. Relationship between $APAR_{green}$, LUE_{green} and GPP proxies

Strong correlations were observed between $APAR_{green}$ and $NIR_{v,Rad}$ (figures 3(a) and (b)). The relationship between $APAR_{green}$ and GPP proxies (figure 3) followed similar time scale patterns as the relationship between GPP and GPP proxies (figure 2). $NIR_{v,Rad}$ showed the strongest correlation with $APAR_{green}$ at all time scales for both corn and soybean. Specifically, for corn, R^2 values of $APAR_{green}$-$NIR_{v,Rad}$ were 0.94, 0.96 and 0.98 at half-hourly, daily and monthly scale, respectively (figure 3(a)), and for soybean, they were

Table 2. RMSE (μmol m^{2} s^{-1}) between tower-based GPP and GPP predicted by NIR$_{v,Rad}$-GPP linear models. Each row refers to a model calibrated at a specific site, and each column refers to different models applied to a specific site.

Calibration sites	Evaluation sites							
	UIUC (rainfed)	UNL (irrigated)	UNL (rainfed)	All sites	UIUC (rainfed)	UNL (irrigated)	UNL (rainfed)	All sites
		Corn				Soybean		
UIUC (rainfed)	9.45	5.94	6.56	8.50	7.20	8.53	4.40	7.29
UNL (irrigated)	10.96	6.89	7.60	9.86	6.90	8.17	4.21	6.98
UNL (rainfed)	9.78	6.14	6.78	8.80	9.16	10.85	5.59	9.27
All sites	9.84	6.18	6.83	8.85	7.70	9.12	4.70	7.79

0.85, 0.83 and 0.91, respectively (figure 3(b)). SIF$_{760}$ also showed similar correlation with APAR$_{green}$ across the three time scales. In contrast, such relationship between APAR$_{green}$ and the two proxies without radiation information (NIR$_{v,Ref}$ and EVI) varied substantially with time scales, following the order of half-hourly < daily < monthly.

We further investigated the relationship between LUE$_{green}$ and NIR$_{v,Ref}$, EVI, LUE$_f$, NIR$_{v,Rad}$/APAR$_{green}$ and LUE$_f$. For corn, NIR$_{v,Rad}$/APAR$_{green}$ had weak correlation with LUE$_{green}$ at half-hourly and daily scales, whereas NIR$_{v,Ref}$, EVI, LUE$_f$ showed no correlation (figure 3(c)). This was probably due to the small seasonal variability of corn LUE$_{green}$ in most of the growing season (figure 1). R^2 values of proxies-LUE$_{green}$ at half-hourly and daily scales were much higher for soybean than for corn (figure 3(d)), and they all increased with time scales, i.e. half-hourly < daily < monthly.

The relationship between GPP and GPP proxies at two UNL sites showed similar time scale patterns (figure S1) as the pattern observed in figures 2(a) and (b) when all site data were used. The above results sufficiently proved that our second hypothesis is correct.

3.3. Relationship between NIR$_{v,Rad}$ and GPP at different sites

The slopes of NIR$_{v,Rad}$-GPP relationship were significantly different between corn and soybean (figure S2). The overall slope was 0.582 (μmol s^{-1} mW^{-1} nm sr) for corn, almost two times of 0.312 (μmol s^{-1} mW^{-1} nm sr) for soybean. There was little variation in slopes of NIR$_{v,Rad}$-GPP relationship for the same crop type across different sites. The cross-site standard deviations of slopes were 0.039 for corn and 0.041 for soybean, with coefficients of variation of 6.6% and 12.9% for corn and soybean, respectively.
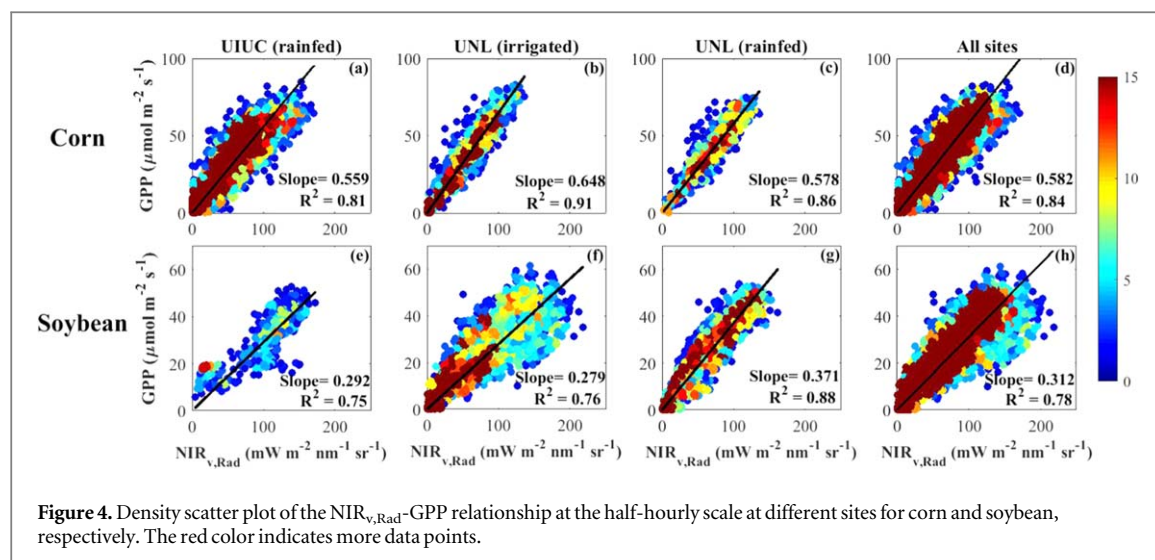
The prediction performance of the NIR$_{v,Rad}$-GPP linear model was relatively stable (table 2), largely confirming our third hypothesis. When the model was calibrated at one site and validated at each of the three sites, the RMSE values were in general within a relatively small range: 6.14 < RMSE < 10.96 for corn, and 4.40 < RMSE < 10.85 for soybean, respectively. Similar small ranges were also observed for R^2 (figure S3) and bias (figure S4), with 0.78 < R^2 < 0.91 and −5.32 < bias < 4.32 for corn, and 0.69 < R^2 < 0.88

and −6.10 < bias < 5.97 for soybean, respectively. Furthermore, when models calibrated at different sites were applied to a specific site, the performance of those models were similar. This was indicated by small RMSE differences (~1 for corn and ~2 for soybean) between different models within each column.

4. Discussion

Our results support all three hypotheses on the NIR$_{v,Rad}$ as a proxy for GPP of corn and soybean. At half-hourly and daily time scales, NIR$_{v,Rad}$ shows considerably higher correlations with GPP than NIR$_{v,Ref}$ and EVI, but they have similar performance at monthly scale (figure 2). At monthly scale, plants adjust their structure and functions to acclimate to environmental changes (Hikosaka and Hirose 1997, Yamori *et al* 2010). As a result, structure and function co-vary with environmental variables, and the reflectance itself is able to capture long-term variability of GPP. In contrast, day-to-day and diurnal variations are strongly affected by high-frequency changes of PAR due to varying solar angle and sky conditions (Peng and Gitelson 2011), which does not cause much changes in bi-directional reflectance (Kim *et al* 2019). Therefore, NIR$_{v,Rad}$ containing the information of PAR in addition to biophysical and biochemical information contained in reflectance-based vegetation indices better captures short-term variability of GPP. SIF$_{760}$ containing considerable PAR information (Miao *et al* 2018) also shows stronger relationship with GPP compared to NIR$_{v,Ref}$ and EVI at half-hourly scale for both species. Though there is a strong link between SIF and GPP at photosystem scale (Porcar-Castell *et al* 2014), SIF$_{760}$ does not show better correlation with GPP than NIR$_{v,Rad}$. A possible reason is the larger uncertainty in SIF observations than reflectance (Meroni *et al* 2009), but more studies are needed to better understand the potential of SIF for estimating GPP.

The strong relationship between NIR$_{v,Rad}$ and GPP is mainly attributed to their strong links with APAR$_{green}$ (figures 3 and S5). A previous study has reported the linear relationship between daily GPP and APAR$_{green}$ for corn and soybean from 2001 through 2008 at the UNL sites (Gitelson *et al* 2015), and we further demonstrate

Figure 4. Density scatter plot of the $NIR_{v,Rad}$-GPP relationship at the half-hourly scale at different sites for corn and soybean, respectively. The red color indicates more data points.

that such linearity is strong at all time scales (figure 3). The dominant role of $APAR_{green}$ in determining GPP variations lies in the fact that LUE_{green} displays small variations during the growth season for both corn and soybean (figure 1). Similar stable LUE values have also been reported at other corn (Campbell *et al* 2019), rice (Yang *et al* 2018a), and wheat sites (Wienforth *et al* 2018). Gitelson *et al* (2018) suggested that crops tend to respond to stress through changes in leaf inclination/leaf rolling which result in decrease of $APAR_{green}$ instead of LUE_{green}. Consequently, $NIR_{v,Rad}$ which captures a majority of $APAR_{green}$ variations serves as a strong proxy for GPP. It is worth mentioning that $NIR_{v,Rad}$ also captures a portion of LUE_{green} variations, whereas SIF does not at half-hourly and daily scales (figure 3). This is due to a negative correlation between LUE_f and LUE_{green} at the early-middle growing season (figure S6). The difference between $NIR_{v,Rad}/APAR_{green}$-LUE_{green} and LUE_f-LUE_{green} explains higher correlation of $NIR_{v,Rad}$-GPP than SIF_{760}-GPP even though $NIR_{v,Rad}$ and SIF_{760} have similar correlation with $APAR_{green}$ (figure 3).

The strong relationship of $NIR_{v,Rad}$-GPP may be further explained by the dominant role of canopy structure. Although LUE is usually considered as a function of leaf physiology which relates to heat and water stress (Running *et al* 2000, Xiao *et al* 2005), its concept is originally based on the functional convergence theory (Monteith 1972, 1977, Field 1991) hypothesizing that plants scale canopy leaf area and light harvesting by the availability of resources as a result of evolutionary processes in order to optimize their carbon fixation (Goetz *et al* 1999). Simulations by sophisticated radiative transfer model also indicate that LUE is a function of canopy structure (Medlyn 1998). A recent ground observation study has provided direct evidence that LUE has a significantly positive correlation with escape ratio of SIF (Dechant *et al* 2019), which captures the effects of canopy structure on observed SIF and can be quantified as the ratio of $NIR_{v,Ref}$ to FPAR (Zeng *et al* 2019). Therefore, it is

reasonable that $NIR_{v,Ref}$ accounts for variations of both FPAR and LUE, and $NIR_{v,Rad}$ agrees well with GPP, given that GPP can be expressed as PAR × FPAR × LUE and $NIR_{v,Rad}$ can be reformed as NIR incoming irradiance × $NIR_{v,Ref}$ under the assumption of Lambertian surface (Schaepman-Strub *et al* 2006) which is similar to PAR × $NIR_{v,Ref}$.

The $NIR_{v,Rad}$-GPP relationship for corn and soybean is site-independent in the US Corn Belt, and the slope of $NIR_{v,Rad}$-GPP is significantly higher for corn than for soybean. The site-independence of $NIR_{v,Rad}$-GPP relationship is revealed from the following two aspects: (1) the slopes between $NIR_{v,Rad}$ and GPP are similar among different sites, though some variations are observed (figure 4); (2) the linear model built at one site can be applied to other sites without significantly losing accuracy (table 2). This is also consistent with a recent study which found a general $NIR_{v,Ref}$-GPP relationship for a wide range of crop sites around the world (Badgley *et al* 2019). The higher slope of $NIR_{v,Rad}$-GPP for corn over soybean is similar as the results from SIF-GPP relationship (Liu *et al* 2017a, Li *et al* 2018) and $NIR_{v,Ref}$-GPP relationship (Badgley *et al* 2019). This is reasonable, as C4 plants tend to have much higher GPP than C3 plants even though they have similar density/greenness. It is worth mentioning that observational factors could influence the generality of the $NIR_{v,Rad}$-GPP relationship. The first one is that the hyperspectral data of this study cover different time periods across sites (table 1). It has been reported that even for a strong proxy-GPP relationship, slope can differ between vegetative and reproductive stages to some degree (Gitelson *et al* 2014). The second one is that Fluospec2 footprint covers less than 2% of EC footprint (Liu *et al* 2017b). Such mismatch between sensor footprints varies across sites and the spatial heterogeneity of underlying surface can further contribute to uncertainties of GPP prediction (Wang *et al* 2019). Further comprehensive studies are

needed to address whether the $NIR_{v,Rad}$-GPP relationship is robust.

The strong and robust $NIR_{v,Rad}$-GPP relationship has a great implication as we can easily apply this relationship at satellite observations to scale up to globe for long-term record or at high resolution. $NIR_{v,Rad}$ is the product of field observed NIR_{Rad} and NDVI. $NIR_{v,Rad}$ can be reformed as:

$$NIR_{v,Rad} = 1/\pi \times NIR_{Irra} \times NDVI \times NIR_{Ref},$$
(9)

where NIR_{irra} is incoming radiation in NIR region and can be derived as the difference between incoming shortwave radiation and PAR, both of which are available from high-resolution satellite data (Ryu *et al* 2018, Hao *et al* 2019) and long-term (>35 year) satellite data (Stackhouse *et al* 2000, Karlsson *et al* 2017). Further, considering both NDVI and NIR_{Ref} are the most fundamental products provided by a large range of satellite platforms (Franch *et al* 2017, Claverie *et al* 2018, Houborg and McCabe 2018), we highlight that the $NIR_{v,Rad}$-GPP relationship has a great potential to be applied to global croplands at a daily interval with spatial resolution up to 3 m (e.g. commercial Planet Labs data) and temporal coverage as far back as 1982 (by the Advanced Very High Resolution Radiometer, AVHRR) with minimum computational cost. Given the understanding of ecosystem's ability to sequestrate carbon becomes more urgent (Keenan *et al* 2016, Ciais *et al* 2019), such scalability opens up huge potentials for real-world applications too (National Academies of Sciences and Medicine E 2019).

5. Conclusion

We investigated the performance of radiance-based NIR_v ($NIR_{v,Rad}$) in estimating GPP of corn and soybean based on field observations across multiple site-years. $NIR_{v,Rad}$ outperformed $NIR_{v,Ref}$, EVI and SIF_{760} for GPP estimation at short timescales (half-hourly and daily), mainly because $NIR_{v,Rad}$ strongly correlated with $APAR_{green}$ which determined GPP variation for both corn and soybean. The $NIR_{v,Rad}$-GPP relationship showed robust performance across sites, indicating that the $NIR_{v,Rad}$-based simple models have a great potential to estimate crop GPP at short timescales with high-resolution or long-term satellite remote sensing data.

Data availability statement

The data that support the findings of this study are available from the corresponding author upon reasonable request.

ORCID iDs

Genghong Wu ⬤ https://orcid.org/0000-0002-6227-6390
Kaiyu Guan ⬤ https://orcid.org/0000-0002-3499-6382
Chongya Jiang ⬤ https://orcid.org/0000-0002-1660-7320
Bin Peng ⬤ https://orcid.org/0000-0002-7284-3010
Hyungsuk Kimm ⬤ https://orcid.org/0000-0001-8189-0874
Carl J Bernacchi ⬤ https://orcid.org/0000-0002-2397-425X
M Pilar Cendrero-Mateo ⬤ https://orcid.org/0000-0001-5887-7890

References

Alonso L, Gómez-Chova L, Vila-Francés J, Amorós-López J, Guanter L, Calpe J and Moreno J 2008 Improved fraunhofer line discrimination method for vegetation fluorescence quantification *IEEE Geosci. Remote Sens. Lett.* **5** 620–4

Anav A *et al* 2015 Spatiotemporal patterns of terrestrial gross primary production: a review *Rev. Geophys.* **53** 785–818

Badgley G, Anderegg L D L, Berry J A and Field C B 2019 Terrestrial gross primary production: using NIR V to scale from site to globe *Glob. Change Biol.* **25** 3731–40

Badgley G, Field C B and Berry J A 2017 Canopy near-infrared reflectance and terrestrial photosynthesis *Sci. Adv.* **3** e1602244

Baker N R 2008 Chlorophyll fluorescence: a probe of photosynthesis in vivo *Annu. Rev. Plant Biol.* **59** 89–113

Bodesheim P, Jung M, Gans F, Mahecha M D and Reichstein M 2018 Upscaled diurnal cycles of land-atmosphere fluxes: a new global half-hourly data product *Earth Syst. Sci. Data* **10** 1327–65

Campbell P K E, Huemmrich K F, Middleton E M, Ward L A, Julitta T, Daughtry C S T, Burkart A, Russ A L and Kustas W P 2019 Diurnal and seasonal variations in chlorophyll

fluorescence associated with photosynthesis at leaf and canopy scales *Remote Sens.* **11** 488

Cendrero-mateo M P *et al* 2019 Sun-induced chlorophyll fluorescence III: benchmarking retrieval methods and sensor characteristics for proximal sensing *Remote Sens.* **11** 962

Chen J M, Ju W, Ciais P, Viovy N, Liu R, Liu Y and Lu X 2019 Vegetation structural change since 1981 significantly enhanced the terrestrial carbon sink *Nat. Commun.* **10** 4259

Ciais P *et al* 2019 Five decades of northern land carbon uptake revealed by the interhemispheric CO_2 gradient *Nature* **568** 221–5

Claverie M, Ju J, Masek J G, Dungan J L, Vermote E F, Roger J-C, Skakun S V and Justice C 2018 The harmonized landsat and sentinel-2 surface reflectance data set *Remote Sens. Environ.* **219** 145–61

Damm A, Guanter L, Paul-Limoges E, van der Tol C, Hueni A, Buchmann N, Eugster W, Ammann C and Schaepman M E 2015 Far-red sun-induced chlorophyll fluorescence shows ecosystem-specific relationships to gross primary production: an assessment based on observational and modeling approaches *Remote Sens. Environ.* **166** 91–105

Dechant B *et al* 2019 Canopy structure explains the relationship between photosynthesis and sun-induced chlorophyll fluorescence in crops *EarthArXiv* (https://doi.org/10.31223/osf.io/cbxpq)

Field C B 1991 Ecological scaling of carbon gain to stress and resource availability *Response of Plants to Multiple Stresses* (New York: Academic) pp 35–65

Franch B *et al* 2017 A 30+ year AVHRR land surface reflectance climate data record and its application to wheat yield monitoring *Remote Sens.* **9** 1–14

Frankenberg C *et al* 2011 New global observations of the terrestrial carbon cycle from GOSAT: patterns of plant fluorescence with gross primary productivity *Geophys. Res. Lett.* **38** 1–6

Gitelson A A, Arkebauer T J and Suyker A E 2018 Convergence of daily light use efficiency in irrigated and rainfed C3 and C4 crops *Remote Sens. Environ.* **217** 30–7

Gitelson A A and Gamon J A 2015 The need for a common basis for defining light-use efficiency: implications for productivity estimation *Remote Sens. Environ.* **156** 196–201

Gitelson A A, Peng Y, Arkebauer T J and Schepers J 2014 Relationships between gross primary production, green LAI, and canopy chlorophyll content in maize: implications for remote sensing of primary production *Remote Sens. Environ.* **144** 65–72

Gitelson A A, Peng Y, Arkebauer T J and Suyker A E 2015 Productivity, absorbed photosynthetically active radiation, and light use efficiency in crops: implications for remote sensing of crop primary production *J. Plant Physiol.* **177** 100–9

Goetz S J, Prince S D, Goward S N, Thawley M M and Small J 1999 Satellite remote sensing of primary production: an improved production efficiency modeling approach *Ecol. Modelling* **122** 239–55

Guanter L *et al* 2014 Global and time-resolved monitoring of crop photosynthesis with chlorophyll fluorescence *Proc. Natl Acad. Sci. USA* **111** E1327–33

Hao D, Asrar G R, Zeng Y, Zhu Q, Wen J, Xiao Q and Chen M 2019 Estimating hourly land surface downward shortwave and photosynthetically active radiation from DSCOVR/EPIC observations *Remote Sens. Environ.* **232** 111320

Hikosaka K and Hirose T 1997 Leaf angle as a strategy for light competition: optimal and evolutionarily stable light-extinction coefficient within a leaf canopy *Écoscience* **4** 501–7

Houborg R and McCabe M F 2018 A cubesat enabled spatio-temporal enhancement method (CESTEM) utilizing Planet, Landsat and MODIS data *Remote Sens. Environ.* **209** 211–26

Jiang C and Ryu Y 2016 Remote sensing of environment multi-scale evaluation of global gross primary productivity and evapotranspiration products derived from breathing earth system simulator (BESS) *Remote Sens. Environ.* **186** 528–47

Joiner J, Guanter L, Lindstrot R, Voigt M, Vasilkov A P, Middleton E M, Huemmrich K F and Yoshida Y 2013 Global monitoring of terrestrial chlorophyll fluorescence from

moderate-spectral-resolution near-infrared satellite measurements: methodology, simulations, and application to GOME-2 *Atmos. Meas. Tech.* **6** 2803–23

Jung M *et al* 2011 Global patterns of land-atmosphere fluxes of carbon dioxide, latent heat, and sensible heat derived from eddy covariance, satellite, and meteorological observations *J. Geophys. Res. Biogeosci.* **116** 1–16

Karlsson K G *et al* 2017 CLARA-A2: the second edition of the CM SAF cloud and radiation data record from 34 years of global AVHRR data *Atmos. Chem. Phys.* **17** 5809–28

Keenan T F, Prentice I C, Canadell J G, Williams C A, Wang H, Raupach M and Collatz G J 2016 Recent pause in the growth rate of atmospheric CO_2 due to enhanced terrestrial carbon uptake *Nat. Commun.* **7** 13428

Kim J, Ryu Y, Jiang C and Hwang Y 2019 Continuous observation of vegetation canopy dynamics using an integrated low-cost, near-surface remote sensing system *Agric. For. Meteorol.* **264** 164–77

Köhler P, Frankenberg C, Magney T S, Guanter L, Joiner J and Landgraf J 2018 Global retrievals of solar-induced chlorophyll fluorescence with TROPOMI: first results and intersensor comparison to OCO-2 *Geophys. Res. Lett.* **45** 10456–63

Li X and Xiao J 2019 Mapping photosynthesis solely from solar-induced chlorophyll fluorescence: a global, fine-resolution dataset of gross primary production derived from OCO-2 *Remote Sens.* **11** 2563

Li X *et al* 2018 Solar-induced chlorophyll fluorescence is strongly correlated with terrestrial photosynthesis for a wide variety of biomes: first global analysis based on OCO-2 and flux tower observations *Glob. Change Biol.* **24** 3990–4008

Liu L, Guan L and Liu X 2017a Directly estimating diurnal changes in GPP for C3 and C4 crops using far-red sun-induced chlorophyll fluorescence *Agric. For. Meteorol.* **232** 1–9

Liu X, Liu L, Hu J and Du S 2017b Modeling the footprint and equivalent radiance transfer path length for tower-based hemispherical *Sensors.* **17** 1–15

Medlyn B E 1998 Physiological basis of the light use efficiency model *Tree Physiol.* **18** 167–76

Meroni M, Rossini M, Guanter L, Alonso L, Rascher U, Colombo R and Moreno J 2009 Remote sensing of solar-induced chlorophyll fluorescence: review of methods and applications *Remote Sens. Environ.* **113** 2037–51

Miao G *et al* 2018 Sun-induced chlorophyll fluorescence, photosynthesis, and light use efficiency of a soybean field from seasonally continuous measurements *J. Geophys. Res. Biogeosci.* **123** 610–23

Monteith J L 1972 Solar radiation and productivity in tropical ecosystems *J. Appl. Ecol.* **9** 747–66

Monteith J L 1977 Climate and the efficiency in Britain climate of crop production *Phil. Trans. R. Soc.* B **281** 277–94

National Academies of Sciences and Medicine E 2019 *Science Breakthroughs to Advance Food and Agricultural Research by 2030* (Washington, DC: The National Academies Press)

Peng Y and Gitelson A A 2011 Application of chlorophyll-related vegetation indices for remote estimation of maize productivity *Agric. For. Meteorol.* **151** 1267–76

Porcar-Castell A, Tyystjärvi E, Atherton J, Van Der Tol C, Flexas J, Pfündel E E, Moreno J, Frankenberg C and Berry J A 2014 Linking chlorophyll a fluorescence to photosynthesis for remote sensing applications: mechanisms and challenges *J. Exp. Bot.* **65** 4065–95

Reichstein M *et al* 2005 On the separation of net ecosystem exchange into assimilation and ecosystem respiration: review and improved algorithm *Glob. Change Biol.* **11** 1424–39

Running S W, Nemani R R, Heinsch F A N N, Zhao M, Reeves M and Hashimoto H 2004 A continuous satellite-derived measure of global terrestrial primary production *Bioscience* **54** 547–60

Running S W, Thornton P E, Nemani R and Glassy J M 2000 Global terrestrial gross and net primary productivity from the earth observing system BT *Methods in Ecosystem Science* ed O E Sala *et al* (New York, NY: Springer New York) pp 44–57

Ryu Y, Berry J A and Baldocchi D D 2019 What is global photosynthesis? History, uncertainties and opportunities *Remote Sens. Environ.* **223** 95–114

Ryu Y, Jiang C, Kobayashi H and Detto M 2018 MODIS-derived global land products of shortwave radiation and diffuse and total photosynthetically active radiation at 5 km resolution from 2000 *Remote Sens. Environ.* **204** 812–25

Schaepman-Strub G, Schaepman M E, Painter T H, Dangel S and Martonchik J V 2006 Reflectance quantities in optical remote sensing-definitions and case studies *Remote Sens. Environ.* **103** 27–42

Sims D A *et al* 2006 On the use of MODIS EVI to assess gross primary productivity of North American ecosystems *J. Geophys. Res. Biogeosci.* **111** 1–16

Stackhouse P W, Gupta S K, Cox S J, Chiacchio M and Mikovitz J 2000 The WCRP/GEWEX Surface radiation budget project release 2: an assessment of surface fluxes at 1 degree resolution *Technical Report* NASA Langley Technical Report Server

Sun Y *et al* 2017 OCO-2 advances photosynthesis observation from space via solar-induced chlorophyll fluorescence *Science* **358** 6360

Suyker A E and Verma S B 2012 Gross primary production and ecosystem respiration of irrigated and rainfed maize-soybean cropping systems over 8 years *Agric. For. Meteorol.* **165** 12–24

van der Tol C, Vilfan N, Dauwe D, Cendrero-Mateo M P and Yang P 2019 The scattering and re-absorption of red and near-infrared chlorophyll fluorescence in the models fluspect and SCOPE *Remote Sens. Environ.* **232** 111292

Wang S, Garcia M, Bauer-Gottwein P, Jakobsen J, Zarco-Tejada P J, Bandini F, Paz V S and Ibrom A 2019 High spatial resolution monitoring land surface energy, water and CO_2 fluxes from an unmanned aerial system *Remote Sens. Environ.* **229** 14–31

Wienforth B, Knieß A, Böttcher U, Herrmann A, Sieling K, Taube F and Kage H 2018 Evaluating bioenergy cropping systems towards productivity and resource use efficiencies: an analysis based on field experiments and simulation modelling *Agron* **8** 117

Xiao X, Zhang Q, Hollinger D, Aber J and Berrien M 2005 Modeling gross primary production of an evergreen forest using MODIS and climate data *Ecol. Appl.* **15** 954–69

Yamori W, Noguchi K, Hikosaka K and Terashima I 2010 Phenotypic plasticity in photosynthetic temperature acclimation among crop species with different cold tolerances *Plant Physiol.* **152** 388–99

Yang K *et al* 2018a Remote sensing of environment sun-induced chlorophyll fluorescence is more strongly related to absorbed light than to photosynthesis at half-hourly resolution in a rice paddy *Remote Sens. Environ.* **216** 658–73

Yang P, Van der Tol C, Verhoef W, Damm A, Schickling A, Kraska T, Muller O and Rascher U 2018b Using reflectance to explain vegetation biochemical and structural effects on sun-induced chlorophyll fluorescence *Remote Sens. Environ.* **231** 110996

Yang X, Tang J, Mustard J F, Lee J E, Rossini M, Joiner J, Munger J W, Kornfeld A and Richardson A D 2015 Solar-induced chlorophyll fluorescence that correlates with canopy photosynthesis on diurnal and seasonal scales in a temperate deciduous forest *Geophys. Res. Lett.* **42** 2977–87

Zeng Y, Badgley G, Dechant B, Ryu Y, Chen M and Berry J A 2019 A practical approach for estimating the escape ratio of near-infrared solar-induced chlorophyll fluorescence *Remote Sens. Environ.* **232** 111209

Zeri M, Anderson-teixeira K, Hickman G and Masters M 2011 Carbon exchange by establishing biofuel crops in Central Illinois *Agric. Ecosyst.s Environ.* **144** 319–29